Structural and optical properties of co-doped ZnO (V, Dy) nanoparticles synthesized by sol-gel

F.F. Al-Harbi
Princess Nourah Bint Abdulrahman University
Jaber EL ghoul (ghoultn@yahoo.fr)
Imam Mohammad Ibn Saud University

Research Article

Keywords: Semiconductors, nano-ZnO, Sol-gel, physical properties

Posted Date: March 31st, 2021

DOI: https://doi.org/10.21203/rs.3.rs-362435/v1

Abstract

In the present work, sol–gel process was used for the synthesisof $Zn_{0.99-x}V_{0.01}Dy_xO$ (x = 0.00, 0.04 and 0.08). We studied the impact of doping on the physical properties of the synthesized nanoparticles. In our synthetic approach, under an esterification reaction the release of water was carried out slowly, this step was followed by drying beyond the critical point of ethanol then by calcination in air at 500°C for 2 hours. The structural and morphological studies show the presence of wurtzite structure with an average crystallite size of about 30 nm. In addition, no secondary phase was detected, which shows that the doping elements reacted with the matrix. The reflectance measurements show that by increasing the doping concentration the energy of the band gap energy decreases. Photoluminescence (PL) indicates the presence of two emission bands situated at at around 481 nm and 577 nm linked to doping with Dy.

1. Introduction

Due to their uses in different application areas such as optoelectronics, photonics and storage devices [1–4], semiconductor nanomaterials have attracted remarkable attention in recent years.ZnO, possessing a vast band gap (3.37 eV) and important exciton binding energy (60 meV), has attracted great attention as a promising material for different applications such as in optoelectronics and electroluminescence [5–8]. Furthermore, its large band gap energy made it animportant candidate as a host lattice for the incorporation of trivalent lanthanide ions due to its exceptional optical properties [9, 10]. The narrow and intense emission lines of the trivalent ions originating from the 4f-4f transitions made them good luminescence centres [11, 12]. The Dy^{3+} ion is one of the lanthanide elements that produce the emission in the visible by activating different inorganic lattices [13, 14]. However, due to the parity forbidden nature of the 4f - 4f transitions of these ions, it has been shown that direct excitation for Dy3 + ions is generally inefficient, unlike the host sensitized [13].To synthesize ZnO doped with lanthanide elements, several methods have been used. Among the different methods, the sol gel method offers certain advantages, in particular an almost uniform size and good dispersion of the dopant.

It is known that the use of ZnO in new magneto-optical applications is difficult because of their diamagnetic and paramagnetic behaviours at room temperature.Room temperature ferromagnetism (RTFM) in ZnO has been reported to result from vacancy mediation [15–17]. Several works have been carried out to improve the RTFM in ZnO by substituting the Zn atom with dopants of transition metals and rare earths. The doping of ZnO to transition metals provides an RTFM linked to the d - d exchange coupling between the non-localized 3d electron and the exterior of the transition metal [18–21]. Whereas the stronger magnetization, relative to transition metals, in the case of doping with rare earth ions is related to the interaction of indirect 4f electron exchange via 5d or 6s conduction electrons [22–25]. Recently, co-doping with two transition metals has enhanced magnetization as was the case of ZnO co-doped Ni, Co, Cu and Fe [26-28]. In recent years, different teams have explored the co-doping of ZnO with a transition metal and rare earth element [29-32].
In this work, we study the vanadium doping jointly with Dysprosium of ZnO nanoparticles prepared by

sol-gel. Therefore, we report the role of these doping elements on the different physical properties of ZnO nanoparticles.

2. Experimental Details

2.1. Preparationdetails

For the synthesis of $Zn_{0.99-x}V_{0.01}Dy_xO$ nanoparticles, we purchased from Sigma-AldrichZinc acetate dihydrate Zn(CH3COO)2·2H2O, ammonium metavanadate (NH4VO3) Dysprosium nitrate hexahydrate Dy(NO3)3·6H2O and Methanol (CH3OH). All our samples were prepared by simple sol–gel route using our approach described in EL GHOUL et al. [33-35].

2.2. Characterization techniques

X-ray diffractograms and transmission electron microscopy images of our sampleswere performed using a diffractometer Bruker D8 with Cu-Kα radiation (λ = 1.5406 Å) and a transmission electron microscope JEM-200CX, respectively. Preparation of samples for TEM is as described abovein EL GHOUL et al. [30, 36]. A SPECS using a PHIBOS100 energy analyzer and Al-Kα radiation (1486.61 eV) was used for the XPS analysis.A RenishawinVia confocal Raman microscope with 785 nm excitation has been used for the Raman measurement. The reflectance measurement was released by aShimadzu UV-3101 PC spectrophotometer coupled with an integrating sphere.Thevalues of band gap energieswereestimatedby usingthe first derivative reflectance method *(dR/dλ)*[37].

3. Results And Discussion

3.1 Structural and morphological analysis

Fig. 1 shows typical XRD spectra of the undoped ZnO and $Zn_{0.99-x}V_{0.01}Dy_xO$ (x=0.00, 0.04 and 0.08) samples. The diffractogramsconfirmthe presence ofpolycrystalline with hexagonal (wurtzite) structure (ICDD file No. 36-1451) with lattice parameters a and c comparable to the undoped ZnO (table 1) [38].No diffraction peak linked to the doping elements appeared, This indicates that the doping is totally successful in the ZnO lattice. We notice, after doping, a small shift towards a larger angle, widening of the peaks and a decrease in the intensity of the peaks compared to ZnO (inset Fig. 1). This is probably linked to the fact that the ionic radii of the present elements are not close {(Zn=0.74Å), (V=0.54 Å) and (Dy=1.03Å)}. Likewise, it can also be due to the introduction of a stress or a defect in the structure of crystal which decreases the crystallinity of the nanoparticles [39].

We used the Williamson-Hall formula to obtain some structural parameters like size and strain of synthesized samplesusing the full width at half height (FWHM) of peak (002) [30].This result is in good harmony with the displacement of the peaks to a higher angles while observing a decrease in the size of the crystallites and strain (Table 1).

The DRX results were confirmed by TEM micrographs of doped samples shown in Fig. 2. These images reveal the presence of a spherical shape with crystallite sizes in the range 25-40 nm.

3.2. Elemental analysis

To know more about the characteristics of the constituent atoms, we used the XPS technique by determining the binding energies of each element. The XPS spectrum of $Zn_{0.95}V_{0.01}Dy_{0.04}O$ sample illustrated in Fig. 3 shows the presence of peaks of the species Zinc, Carbon, Oxygen, Vanadium and Dysprosium. Zinc and oxygen appear with Zn 2p1/2 and Zn 2p3/2 valance states located at 1044.20, 1022.21 eV and asymmetric O1s at 532 eV, respectively.

The dysprosium element is represented by the 4d valance state located at 156.09 eV. The appearance of this peak is a signal indicating that the Dy ion is with oxidation state Dy+3 [40]. The peak located at 517.8 eV corresponds to the V 2p signal and confirms that it is probably present in the V5+ state [41]. From this, we can conclude that Dy and V are successfully doped into ZnO.

3.3 Raman analysis

The chemical structure of the $Zn_{0.91}V_{0.01}Dy_{0.08}O$ nanoparticles was approved by the Raman analysis and illustrated in Fig. 4.It is known that the active modes A1, E1 can move into longitudinal (LO) and transverse (TO) optical modes. The E1 (LO) is related to lattice defects, while B1 modes are considered as inactive Raman and infrared modes [42]. On the other hand, the vibrations of the oxygen and zinc elements in the lattice induce the presence of the sub-modes of E2 high and E2 low [43].This spectrum shows the presence of different acoustic and optical modes which are known in the Wurtzite lattice [42]. The peaks around 660cm-1, 430 cm-1 and 370 cm-1 are assigned to the two-phonon processes A1 (LO) + E2 (low), vibration mode E2 (high) and transverse optical phonon mode E1 (TO), respectively [42, 4445, 43].We observe the appearance of some peaks corresponding to the optical phonon mode of ZnO as B1(low) silent and A1(TO) modes, in the range 220-350 cm^{-1}.The existence of these types of modes is probably related to the effects of different defects such as V_o and Zn_i. On the right side of the spectrum, the appearance of certain peaks could be a sign of the presence of V doping impurity phases [42, 44].

3.3 Optical properties

The reflectance spectra illustrated in Fig. 5 approves characteristics of nano-ZnO, showing a low reflectance in the UV spectral range and high reflectance in the visible domain.

The plot of the first derivative of the reflectance (dR/dλ) as a function ofλ, as shown in Fig. 6, present a shift towards high wavelengths, that is to say a decrease in band gap value afterdoping. We suggest that the band gap drop can be attributed to the effect of doping elements in the host lattice [46].

3.4 Photoluminescence (PL)

Figure 7 shows the PL spectra of $Zn_{0.99-x}V_{0.01}Dy_xO$ (x=0.00, 0.04 and 0.08) nanoparticles excited with 330 nm at room temperature. The PL studies show that the appearance of a band-edge emission occurs at 380 nm for the $Zn_{0.99}V_{0.01}O$ which shifts to the red after Dy doping, confirming the decrease in the bandgap. In addition, the PL spectra consist of two others bands centered at around 481 nm and 577 nm which are attributed to the transitions $^4F_{9/2}\rightarrow{}^6H_{15/2}$ and $^4F_{9/2}\rightarrow{}^6H_{13/2}$, respectively [47]. No significant change in the position or shape of the bands was manifested with the increase in the concentration of Dy^{3+}. This amounts to the protection of the 4f electrons by the outer 5s and 5p electrons.

The two transitions $^4F_{9/2}\rightarrow{}^6H_{15/2}$ and $^4F_{9/2}\rightarrow{}^4H_{13/2}$ are ascribed to a magnetic andforced electric dipole transitions, respectively. The crystal field strength of host matrix does not strongly affect the transition to the $^6H_{15/2}$ level, while that the one towards $^4H_{13/2}$ level is hypersensitive to the surroundings. We have noticed that the spectral intensity of the $^4F_{9/2}\rightarrow{}^4H_{13/2}$ transition higher than the $^4F_{9/2}\rightarrow{}^6H_{15/2}$ transition. This is due to the localization of Dy^{3+} ions on sites of low symmetry without centers of inversion. A large interaction between the host matrix and the RE ion is induced by asymmetry when the intensity of the hypersensitive transition is high [48]. Fig. 8 shows the energy level diagram of Dy^{3+} doped ZnO:V. As the excitation energy (330 nm) is greater than the energy of 4F9/2 level (475nm), the excess energy lost through non-radiative channels. This produces the radiative emission of the populated level $^4F_{9/2}$.

4. Conclusions

$Zn_{0.99-x}V_{0.01}Dy_xO$ nanopowders were prepared by sol-gel route. XRD and TEM analysis show the presence ofpolycrystalline wurtzite structure and average crystallite size around 30nm. The absorbance shows a red shift after doping, indicating the decrease of the band gap due to creation of defects in the band gap.The photoluminescence study shows the existence of two emission peaks centered at around 481 nm and 577 nm linked to the effect of co-doping by Dy and confirming the absorption results. We suggest that these emissions peaks are related to the transitions $^4F_{9/2}\rightarrow{}^6H_{15/2}$ and $^4F_{9/2}\rightarrow{}^6H_{13/2}$, respectively. These results confirm the good synthesize of our samples and offer major advantage for theirs use in optoelectronic domain.

Declarations

Acknowledgment

This research was funded by the Deanship of Scientific Research at Princess Nourah bint Abdulrahman University through the Fast-track Research Funding program.

References

[1] K. Ellmer, A. Klein, Springer Berlin Heidelberg, 104 (2008) 1.

[2] S. Calnan, A.N. Tiwari, Thin Solid Films 518 (2010) 1839.

[3] J. El Ghoul. J Mater Sci-Mater Electron. 27 (2016) 2159.

[4] A. Janotti, C.G. Van de Walle, Rep. Prog. Phys. 72 (2009) 126501.

[5] J. El Ghoul, N. Bouguila, S.A. Gómez-Lopera, L. El Mir, Superlattices and Microstructures, 64 (2013) 451.

[6] M. Mehrabian, R. Azimirad, K. Mirabbaszadeh, H. Afarideh, M. Davoudian, Phys E 43 (2011) 1141.

[7] M. Willander, O. Nur, J. R. Sadaf, M. I. Qadir, S. Zaman, A. Zainelabdin, N. Bano, and I. Hussain, Materials 3 (2010) 2643.

[8] M. Willander, O. Nur, Q. X. Zhao, L. L. Yang, M. Lorenz, B. Q. Cao, J. Z. Perez, C. zekalla, G. Zimmermann, M. Grundmann, A. Bakin, A. Behrends, M. Al-Suleiman, A. El-Shaer, A. C. Mofor, B. Postels, A. Waag, N. Boukos, A. Travlos, H. S. Kwack, J. Guinard, D. L. Dang, Nanotechnology 20 (2009) 332001.

[9] A. Ishizumi, Y. Kanemitsu, Appl Phys Lett 86 (2005) 253106.

[10] Y. Liu, W. Luo, R. Li, X. Chen, Opt Lett 32 (2007) 566.

[11] L. Armelao, G. Bottaro, M. Pascolini, M. Sessolo, A. Tondello, J Phys Chem C 112 (2008)4049.

[12] S. Taguchi, A. Ishizumi, T. Tayagaki, Y. Kanemitsu, Appl Phys Lett 94 (2009) 173101.

[13] Y. Liu, R. Li, W. Luo, H. Zhu, X. Chen, Spectrosc Lett 43 (2010)343.

[14] G. S. Wu, Y. L. Zhuang, Z. Q. Lin, X. Y Yuan, T. Xie, L. D. Zhang Phys E 31 (2006) 5.

[15] E.Z. Liu, Y. Liu, J.Z. He, Appl. Phys. Lett. 93 (2008) 132506.

[16] D. Kim, J. Yang, J. Hong, J. Appl. Phys. 106 (2009) 013908.

[17] B. Chen, Q.X. Yu, Q.Q. Gao, Y. Liao, G.Z. Wang, Appl. Phys. Lett. 102 (2013) 132405. [18] A. Kaushik, B. Dalela, R. Rathore, V.S. Vats, B.L. Choudhary, P.A. Alvi, S. Kumar, S. Dalela, J. Alloys Compd. 578 (2013) 328.

[19] J.A. Wibowo, N.F. Djaja, R. Saleh, Adv. Mater. Phys. Chem. 3 (2013) 48.

[20] S. Kumar, C.L. Chen, C.L. Dong, Y.K. Ho, J.F. Lee, T.S. Chan, R. Thangavel, T.K. Chen, B.H. Mok, S.M. Rao, M.K. Wu, J. Mater. Sci. 48 (2013) 2618.

[21] P. Kaur, S.K. Pandey, S. Kumar, N.S. Negi, C.L. Chen, S.M. Rao, M.K. Wu, Appl. Nano 5 (2015) 975.

[22] P. P. Murmu, J. Kennedy, B. J. Ruck, G.V.M. Williams, A. Markwit, S. Rubanov, A. A. Suvorova, J. Mater. Sci. 47 (2012) 1119.

[23] S. Kumar, P. Kaur, C.L. Chen, R. Thangavel, C.L. Dong, Y.K. Ho, J.F. Lee, T.S. Chan, T.K. Chen, B.H. Mok, S.M. Rao, M.K. Wu, J. Alloys Compd. 588 (2014) 705.

[24] S. Kumar, R. Thangavel, Elec. Mater. Lett. 13 (2017) 129.

[25] P. Kaur, S. Kumar, C.L. Chen, Y.Y. Hsu, T.S. Chan, C.L. Dong, C. Srivastava, A. Singh, S.M. Rao, Appl. Phys. A 122 (2016) 1.

[26] Z.F. Wu, K. Cheng, F. Zhang, R.F. Guan, X.M. Wuc, L.J. Zhuge, J. Alloys Compd. 615, (2014) 521.

[27] S. Chattopadhyay, T.K. Nath, A.J. Behan, J.R. Neal, D. Score, Q. Feng, A.M. Fox, G.A. Gehring, J. Magn. Magn. Mater. 323 (2011) 1033.

[28] L. Liu, P.Y. Yu, Z. Ma, S.S. Mao, Phys. Rev. Lett. 100 (2008) 127203.

[29] Q. Xu, H. Schmidt, H. Hochmuth, M. Lorenz, A. Setzer, P. Esquinazi, C. Meinecke, M. Grundmann, J. Phys. D: Appl. Phys. 41 (2008) 105012.

[30] J. El Ghoul, F.F. Al-Harbi, Journal of Inorganic and Organometallic Polymers and Materials,*JInorgOrganometPolym* (2020). https://doi.org/10.1007/s10904-020-01678-4

[31] M.H.N. Assadi, Y.B. Zhang, P. Photongkam, S. Li, J. Appl. Phys. 109 (2011) 013909.

[32] H. Huang, Y. Ou, S. Xu, G. Fang, M. Li, X.Z. Zhao, Appl. Surf. Sci. 254, (2008) 2013.

[33] J. El Ghoul, C. Barthou, L. El Mir, Physica E 44 (2012) 1910.

[34] J. El Ghoul, C. Barthou, L. El Mir, J. Superlattices Microstruct. 51 (2012) 942.

[35] J. El Ghoul, C. Barthou, M. Saadoun, L. El Mir, J. Phys. B 405 (2010) 597.

[36] J. El Ghoul, F.F. Al-Harbi, Solid StateCommunications314–315 (2020) 113916.

[37] S. Mourad, J. El Ghoul, K.Omri, K. Khirouni, CHINESE PHYSICS B 28,047701 (2019) 4 .

[38]Powder Diffraction File, Joint Committee for Powder Diffraction Studies (JCPDS) File No. 36-1451.

[39] T. Thangeeswari, P.Murugasen, J.Velmurugan. J. Supercond. Nov. Magn. 28 (2015) 2505.

[40] F. Zhan, Y. Yang, W. Li, J. Li, W. Liu, Y. Li, Q. Chen, RSC Adv. 6 (2016) 10393.

[41] L. Zhang, D.R. Chen, X.L. Jiao, J. Phys. Chem. B 110 (2006) 2668.

[42] M. M. Obeid, H. R. Jappor, K. Al-Marzoki, I. A. Al-Hydary, Sh. J. Edrees and M. M. Shukur. RSC Adv., 9 (2019) 33207.

[43] V. Russo, M. Ghidelli, P. Gondoni, C.S. Casari, A. Li Bassi, J. Appl. Phys. 115 (2014) 073508.

[44] C. Lung, M. Toma, M. Pop, D. Marconi, A. Pop. Journal of Alloys and Compounds 725 (2017) 1238.

[45] Carlos Batista, Vasco Teixeira, J.O Carneiro. Journal of Nano Research 2(2008) 21.

[46] S. Thaslin, N. Fathima, A. Anandhan, A.R.K.P. Ganesan, M. Karthikeyan, T. Marimuthu, IRJET 4 (2017) 89.

[47] J.S. Kumar, K. Pavani, A.M. Babu, N.K. Giri, S.B. Rai, L.R. Moorthy, J. Lumin. 130(2010) 1916.

[48] J.B. Gruber, B. Zandi, U.V. Valiev, S.A. Rakhimov, J. Appl. Phys. 94 (2003)1030.

Table

Table (1): Variation of different physical parameters for all samples.

Sample	a (Å)	C (Å)	Crystallite size (nm)	Strain (ε) $* 10^{-4}$	Bandgap (eV)
Undoped ZnO	3.2498	5.2063	34.71	1.59	3.333
x=0.0	3.2497	5.2063	32.84	1.48	3.315
X=0.04	3.2494	5.2064	29.73	1.39	3.287
X=0.08	3.2495	5.2065	27.38	1.31	3.246

Figures

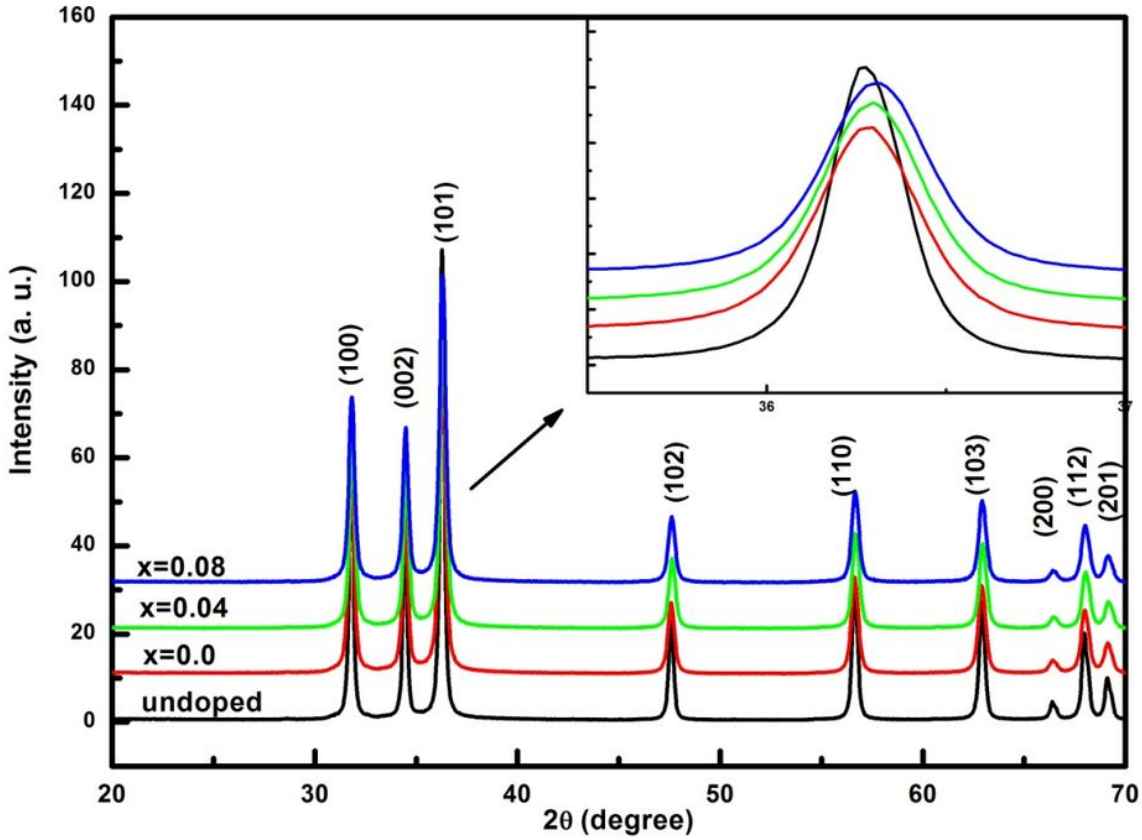

Figure 1

XRD patterns of undoped and Zn0.99-xV0.01DyxO (x=0.00, 0.04 and 0.08) nanoparticles. The inset shows the loop of the (101) diffraction peak.

Fig.2

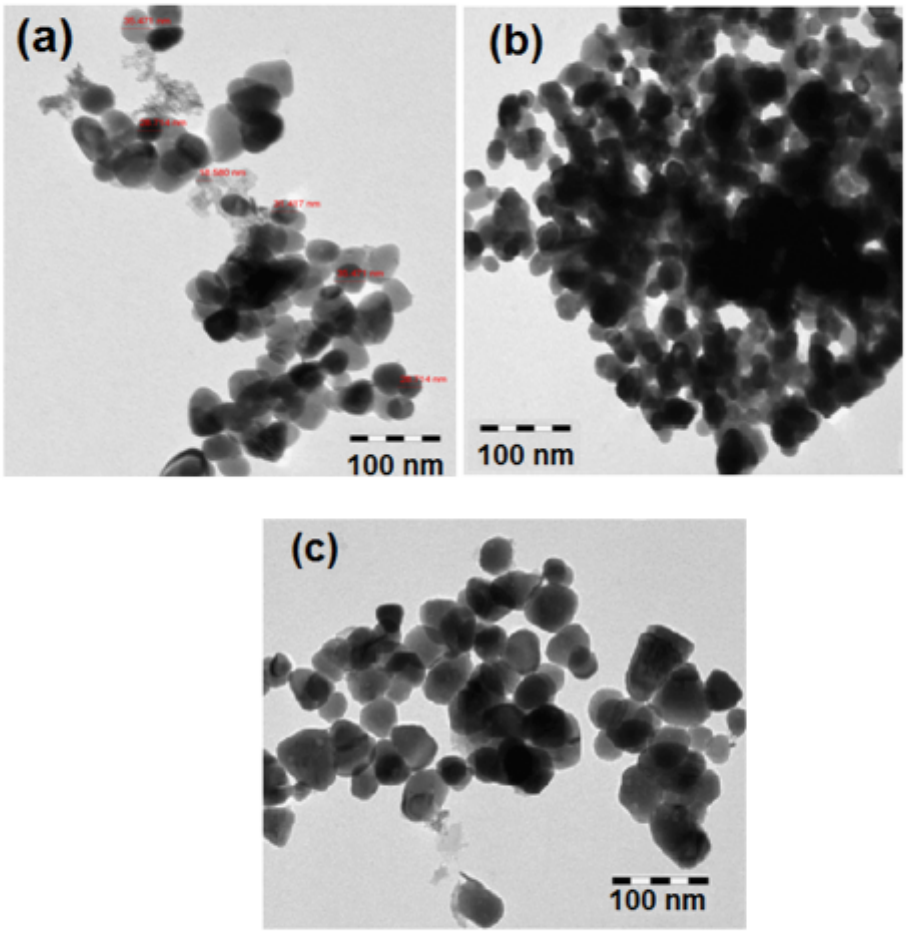

Figure 2

TEM images of (a) Zn0.99V0.01O, (b) Zn0.95V0.01Dy0.04O and (c) Zn0.91V0.01Dy0.08O nanoparticles.

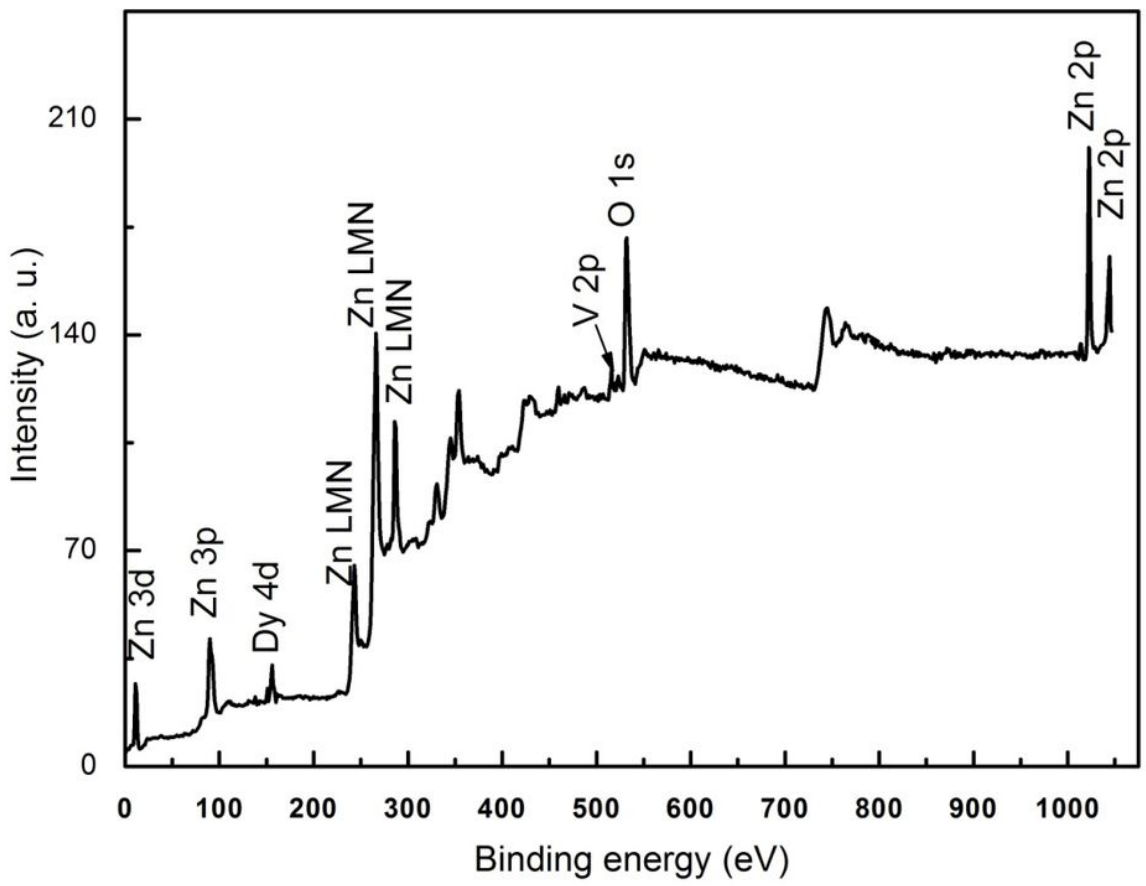

Figure 3

XPS spectrum of Zn0.95V0.01Dy0.04O nanoparticles.

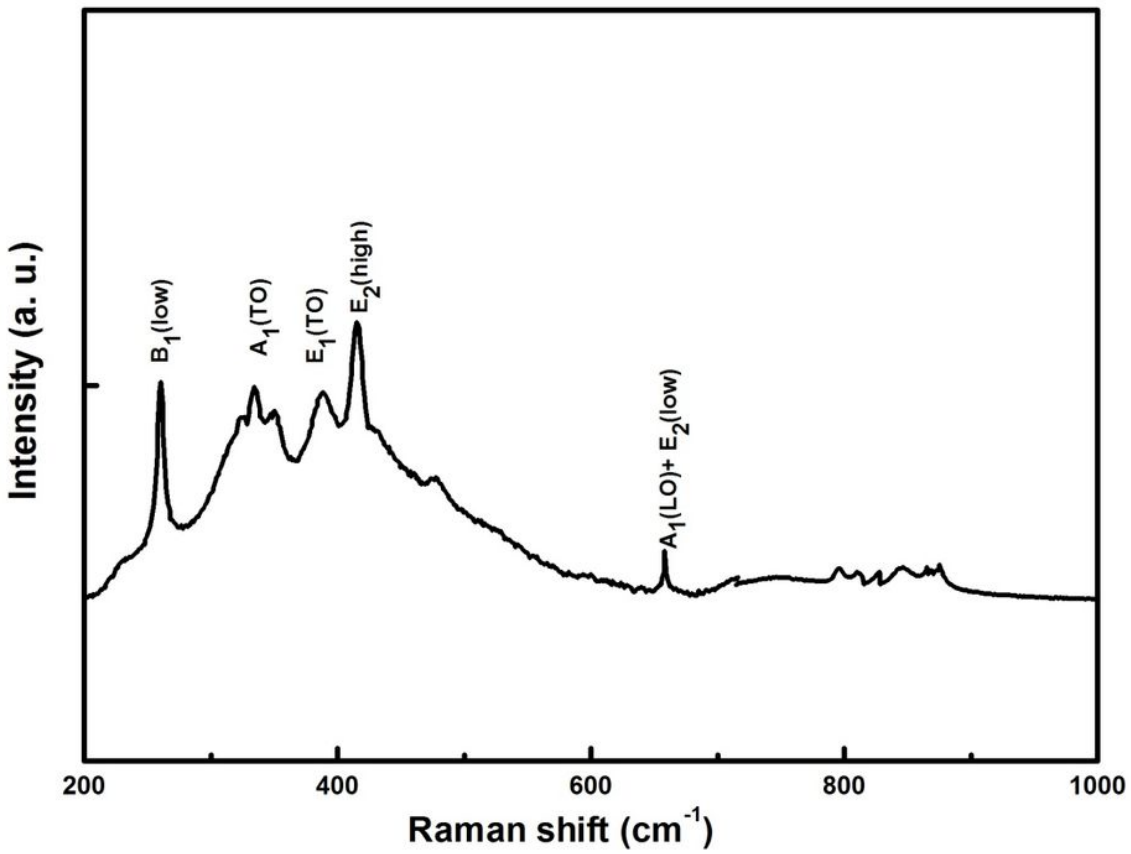

Figure 4

Raman spectrum of Zn0.95V0.01Dy0.04O nanoparticles.

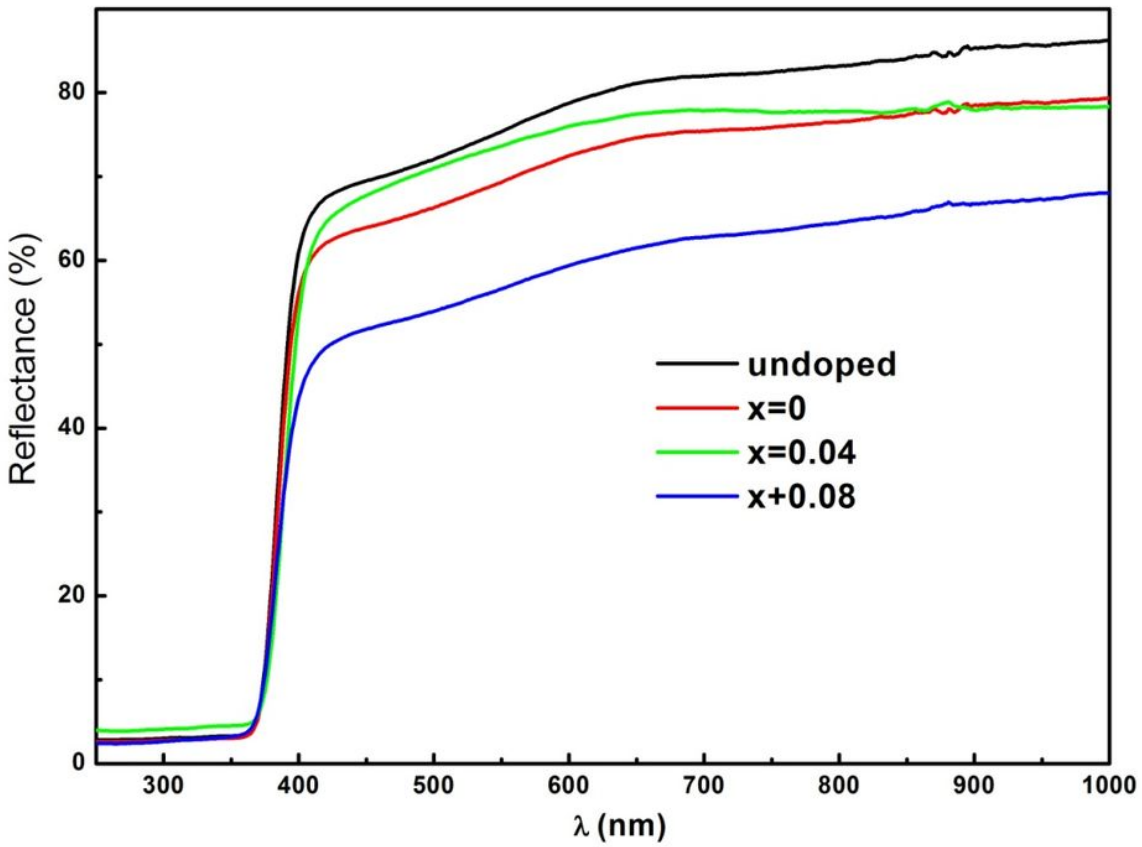

Figure 5

Reflectance spectra of undoped and Zn0.99-xV0.01DyxO (x=0.00, 0.04 and 0.08) nanoparticles.

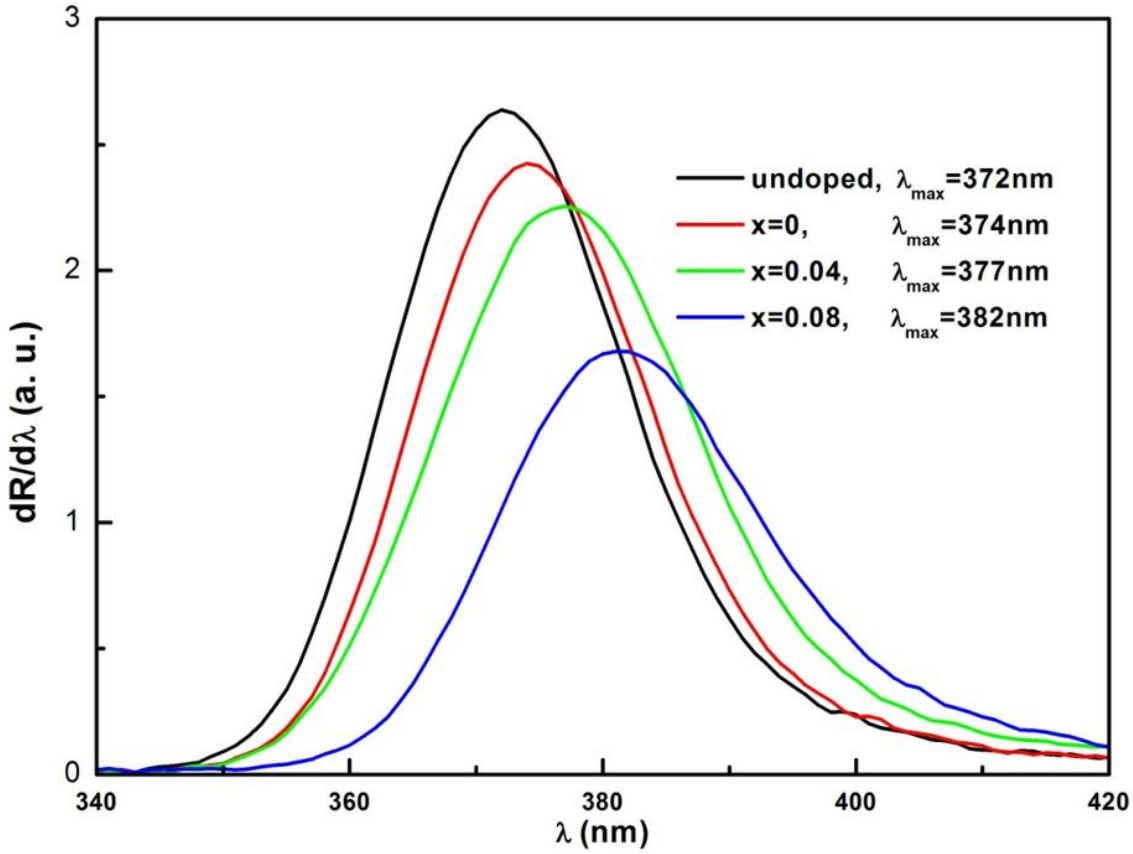

Figure 6

First derivative of the reflectance (dR/dλ) vs. λ of undoped and Zn0.99-xV0.01DyxO (x=0.00, 0.04 and 0.08) nanoparticles.

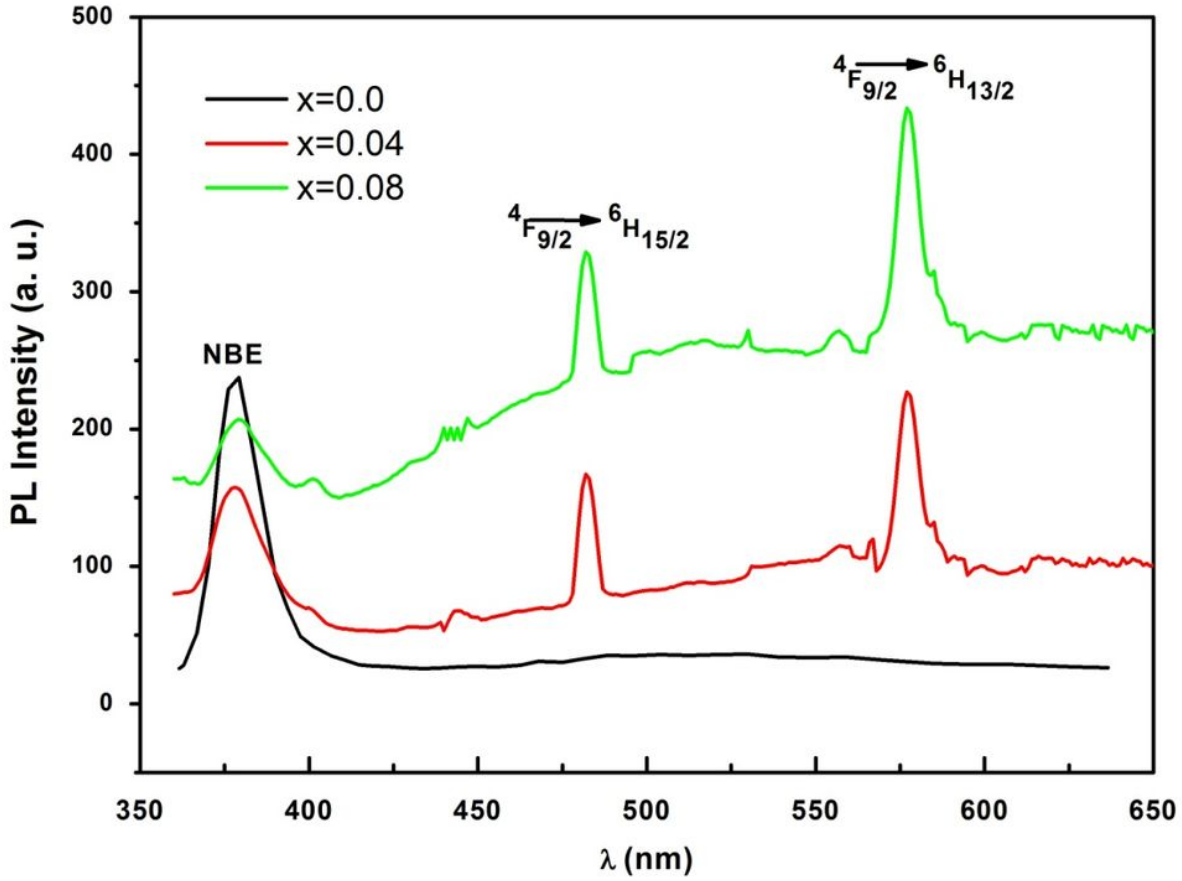

Figure 7

PL spectra of Zn0.99-xV0.01DyxO (x=0.00, 0.04 and 0.08) nanoparticles.

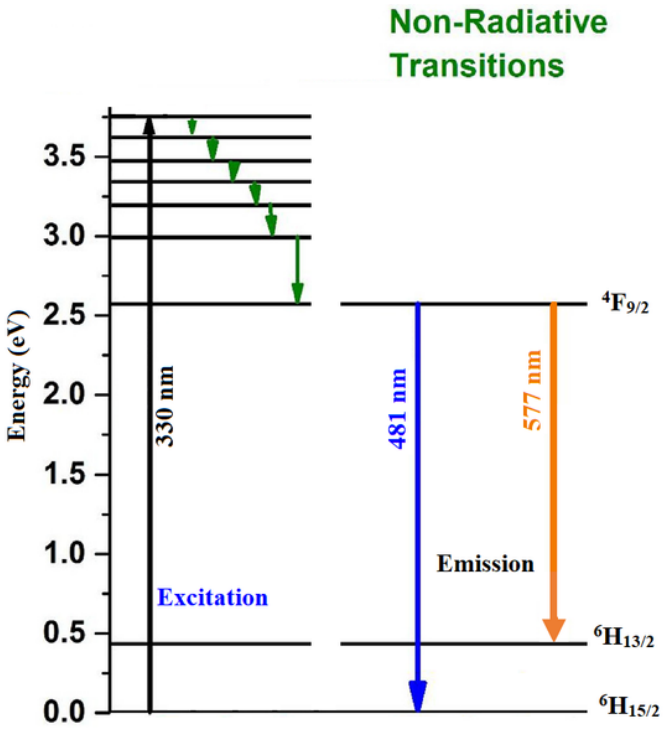

Figure 8

Energy level diagram of Dy3+ doped ZnO:V.